Microanalysis of S, Cl, and Br in fluid inclusions by LA-ICP-MS

Author(s):
Seo, Jung Hun; Guillong, Marcel; Aerts, Maarten; Zajacz, Zoltán; Heinrich, Christoph A.

Publication date:
2011-05

Permanent link:
https://doi.org/10.3929/ethz-b-000037746

Originally published in:
Chemical Geology 284(1-2), https://doi.org/10.1016/j.chemgeo.2011.02.003

This is the Green Open Access version of: Seo, J. H., Guillong, M., Aerts, M., Zajaz, Z., Heinrich, C. A., 2011. Microanalysis of S, Cl, and Br in fluid inclusions by LA-ICP-MS. *Chemical Geology*, Vol. 284, pp. 35-44.
Original publication see: https://doi.org/10.1016/j.chemgeo.2011.02.003

Microanalysis of S, Cl, and Br in fluid inclusions by LA-ICP-MS

Jung Hun Seo[1], Marcel Guillong[1,2], Maarten Aerts[1,3], Zoltan Zajacz[4], and Christoph A. Heinrich[1,5]

1. Institute of Geochemistry and Petrology, ETH Zurich, 8092 Zurich, Switzerland
2. CODES, University of Tasmania, Private Bag 79, Hobart, Australia 7001
3. Natural History Museum, University of Oslo, P.O: Box 1172, Blindern, NO-0318 Oslo, Norway
4. Laboratory for Mineral Deposits Research, Department of Geology, University of Maryland, College Park, MD 20742, USA
5. Faculty of Mathematics and Natural Sciences, University of Zurich, Switzerland

Corresponding author: Jung Hun Seo
Affiliation (Institute of Geochemistry and Petrology, ETH Zurich, Switzerland)
E-mail (seo@erdw.ethz.ch)
Phone (+41-079-309-4768)
Fax (+41-44-632-1827)
Address (NW F 82.1, Clausiusstrasse 25, 8092 Zurich, Switzerland)

Abstract

The accuracy and precision of micro-analysis of sulfur (S), chlorine (Cl) and bromine (Br) in quartz-hosted fluid inclusions by laser ablation (LA) inductively coupled plasma mass spectrometry (ICP-MS) was tested. A scapolite mineral sample (Sca17) can be used as standard reference material (SRM) for the determination of Cl and Br, and NIST610 glass for S determination in fluid inclusions. We found that laser ablation of quartz and UV irradiation in the ablation cell produced elevated background signals of S and to a lesser amount of Cl and Br due to remobilization of these elements from the inside surfaces of the ablation

chamber. Careful cleaning of the ablation chamber with nitric acid and by UV irradiation results in a 10 times lower S contamination signal and improves fluid inclusion analysis by reducing the detection limit for S by 50%. Micro-analysis of liquid and vapor inclusions synthesized in two different laboratories produce good accuracies of S, Cl, and Br. Analytical uncertainties based on numerous analyses of individual synthetic fluid inclusions in one assemblage are 17 – 44 % (RSD) for the sulfur concentration, and 6 – 26 % for Br/Cl ratios. Limits of detection (LOD) in 30 µm diameter liquid inclusions with densities of 0.99-1.02 g/cm^3 are in the range of 60 µg/g for S, 250 µg/g for Cl, and 15 µg/g for Br. LOD's in similar sized vapor inclusions with a density of 0.33 g/cm^3 are at least an order of magnitude poorer. Based on the investigated natural brine inclusion assemblages, the precisions of Br/Cl ratios (4 - 9 % RSD) is adequate to determine the source of salinity in different ore-forming fluids.

Keywords: LA-ICP-MS, fluid inclusion, sulfur, chlorine, bromine, halogen

1. Introduction

Anion components of sulfur, chlorine, and bromine contained in terrestrial fluids including seawater, groundwater, sedimentary formation water, deep subduction fluids, and magmatic-hydrothermal fluids are important for many geochemical aspects in a variety of geological processes (Burgess et al., 2002; Davis et al., 1998; Foriel et al., 2004; Jambon et al., 1995; Sumino et al., 2010; Villemant and Boudon, 1999). For example, sulfate, chlorine, and bromine and their ratios are indicators of bio-availabilities and secular variations of paleo-ocean evolution (Foriel et al., 2004; Van Kranendonk, 2006). In ore-forming hydrothermal fluids, sulfur is an important element controlling pH, redox-state (Ohmoto and Lasaga, 1982; Webster and Mandeville, 2007), and the transport of gold and in part copper operating as a key ligand (Cauzid et al., 2007; Crerar and Barnes, 1976; Etschmann et al., 2010; Heinrich et al., 2004; Nagaseki and Hayashi, 2008; Pokrovski et al., 2008; Seo et al., 2009; Stefansson and Seward, 2004; Zajacz and Halter, 2009; Zajacz et al., 2010). Precipitation of sulfide minerals such as chalcopyrite ($CuFeS_2$), molybdenite (MoS_2), galena (PbS_2), sphalerite ($ZnFeS_2$), and pyrite (FeS_2) require the presence of sulfur in the hydrothermal fluids (Wood and Samson, 1998). Chlorine is an important element in ore-forming fluids as a complexing ligand for metals such as Fe, Mn, Pb, Zn, and Ag (Seward and Barnes, 1997; Wood and Samson, 1998; Yardley, 2005). The Br/Cl ratio can be used as a tracer for the source of chloride in saline fluids and the possible involvement of evaporites, as the two elements primarily fractionate between natural brines and halite (Baker et al., 2008; Bohlke and Irwin, 1992a; Bohlke and Irwin, 1992b; Braitsch, 1971; Heinrich et al., 1993; Holser, 1983; Kharaka et al., 1987; Nahnybida et al., 2009; Stoffell et al., 2008;

Wilkinson et al., 2005).

For the determination of sulfur, chlorine, and bromine in fluid inclusions, bulk extraction methods (Banks and Yardley, 1992; Bray and Spooner, 1992) are commonly used, but such results generally average several generations of inclusions, making interpretation of detailed geological history difficult. Quantitative analyses of anions in individually selected, single fluid inclusion when present at high concentrations has been shown to be possible by micro proton-induced X-ray emission (μ-PIXE) (Baker et al., 2008; Heinrich et al., 1992; Ryan et al., 1993) and by synchrotron X-ray fluorescence (s-XRF) (Cauzid et al., 2007; Foriel et al., 2004), but precision is limited by the partial overlap of the S and Cl peaks, hampering the sensitivities of sulfur detection. Moreover, absorption of low-energy X-ray photons in the host material requires fluid inclusions with well defined geometry that are less than 10 μm below the sample surface, to get reasonable detection limits and reliable quantification. Typical detection limits of 0.1 – 1% S in normal (20-50 μm) inclusions can be obtained by μ-PIXE technique (Ryan et al., 1993). With a minimum uncertainty of 30% in single inclusion analysis by μ-PIXE technique (Heinrich et al., 1992) and the expense of obtaining data from numerous inclusions for statistical improvement of the results, it is difficult to discriminate Br/Cl variations among high temperature magmatic-hydrothermal ore fluids, which so far have been regarded in the range of "magmatic Br/Cl atomic ratios" of around 1-5 * 10^{-3} (Baker et al., 2008).

Laser ablation (LA) ICP-MS is now established as a cost-effective, fast and sensitive method suitable for multi-element analysis in fluid inclusions (Gunther et al., 1998; Heinrich et al., 2003). Recently, we developed a technique to determine the sulfur concentrations in single fluid inclusions (Guillong et al., 2008a) and obtained essential information on the role of S in high temperature magmatic-hydrothermal fluids (Seo et al., 2009). The biggest challenge for the analysis of the anions by LA-ICP-MS is posed by their high first ionization potentials (S: 10.36 eV, Cl: 12.97 eV, Br: 11.81 eV) which are close to that of the Ar (15.76 eV) plasma source, resulting in relatively low sensitivities. In addition, polyatomic isobaric interferences (e.g. $^{16}O^{16}O^{+}$) from ambient air result in high gas background on all sulfur isotopes. Finally, an unknown S contamination resulting in artificially enhanced S signal during UV laser ablation has been described (Guillong et al., 2008a). This work also showed that the S qunatification in fluid inclusions by ICP quadruple MS is not primarily limited by its O_2 interference, by comparing result with ICP high resolution MS analysis. Finally a careful correction of host signals is given to account for the unknown S contamination during ablation (Guillong et al., 2008a).

In this work, we further test and minimize these sources of uncertainty, based on analyses of synthesized fluid inclusions containing known element concentrations. The accuracy,

precision, and detection limits of sulfur, as well as chlorine, and bromine analyses of singly-targeted fluid inclusions by LA-ICP-MS are evaluated, including initial geological applications.

2. Methods

2.1. Instrument Setup

An ICP-Quadrupole-MS (Perkin Elmer Elan 6100 DRC) is connected to the ETH prototype for the GeoLas laser ablation system (193 nm ArF excimer laser) (Gunther et al., 1997). The mass spectrometer was optimized for the detection of sulfur, chlorine, and bromine regarding dry gas backgrounds and sensitivities, while maintaining multi element capability for the simultaneous measurement of additional metals of interest. Addition of a small amount of H_2 gas (5 ml/min.) into the He carrier stream increases the sensitivity of most elements, in particular for some economically important metals such as Cu, Au, and Mo (Guillong and Heinrich, 2007), without impairing S, Cl and Br analysis. A reduced set of measured isotopes (^{23}Na, ^{29}Si, ^{32}S, ^{35}Cl, ^{85}Rb, ^{79}Br, ^{133}Cs) with increased dwell times on selected elements (20 ms on ^{32}S, 40 ms on ^{35}Cl, and 60-80 ms on ^{79}Br) reduces the uncertainty of the background measurements and yields better limits of detection for the elements of interest. Gas blanks on mass 32 ranges from 50'000 to 80'000 count per second (cps) (from ^{16}O^{16}O and ^{32}S in ambient air, He carrier and Ar plasma gas; Guillong et al., 2008a), from 2'000 to 3'000 cps on mass 35 (Cl from contamination of ablation chamber, ambient air, and He carrier gas, and formations of minor ^{16}O^{18}OH, ^{16}O^{17}OHH), and from 2'000 to 3'000 cps on mass 79 (Br from contamination of ablation chamber, ambient air, and He carrier gas, and formation of minor ^{40}Ar^{38}ArH).

The laser energy density was selected between 30 and 40 J/cm^2 with 10 Hz repetition rate to produce controlled sampling of quartz-hosted fluid inclusions. An iris aperture is gradually opened during each analysis from 10 μm up to a spot size suitable for complete excavation of the fluid inclusion. We used a self-built small volume (1 cm^3) aluminum ablation cell containing no organic materials, except for an O-ring that is largely hidden in a groove below the top glass cover. Details of the instrumental setup are summarized in the Table 1.

2.2. Standard Reference Materials (SRM) and Data Reduction

SRM 610 from NIST (NIST610) glass is used as standard reference material for S (550 ± 40 μg/g), which has previously been quantified by LA-ICP-HR-MS using a well characterized (EPMA) scapolite as primary reference (Guillong et al., 2008a). Sulfur analyses of two different sulfur-bearing minerals, a scapolite (Sca17) and an afghanite (AfgAA), in

combination with NIST610 glass and optical grade fused silica were used to validate the calibration curve for S (Figure 1). Reference values were determined by EPMA at ETH Zurich (ETHZ), University of Tasmania (UTAS), and University of Bayreuth (Bayreuth) for Sca17 (Si: 26.2 ± 0.3 wt%, S: 2'900 ± 500 □g/g) and AfgAA (Si: 14.9 ± 0.3 wt%, S: 43'000 ± 4'000 □g/g). For EPMA S quantifications of Sca17 and AfgAA by EPMA, we used stoichiometries of pure minerals of pyrite (ETHZ), marcasite (UTAS), and barite (Bayreuth) as external SRM. For EPMA analyses at UTAS. NIST610 value is taken from the literature (Guillong et al., 2008a) and the S concentration in optical grade fused silica is assumed to be 0 (validated by bulk XRF). The resulting linear calibration curve for the S/Si ratio shows internal consistency so that any of the investigated sulfur-bearing materials can be used for sulfur quantification (Figure 1).

Table 1. Instrumental parameters of the LA-ICP-MS system used in this study.

Laser system type	Beam homogenized ArF excimer system (ETH prototype)
Wavelength	193 nm
Ablation chamber	In house bulit small volume (aluminum, 1 cm^3)
Energy density for quartz ablation	more than 30 J/cm^2
Repetition rate	10 Hz
Crater size for FI analysis	Gradually increase up to FI size by Iris aperture
ICP-MS	Perkin Elmer Elan 6100 DRC
Carrier gas flow	1.10-1.15 l/min He
Additional gas flow	5 ml/min H_2
Make up gas flow	0.8-0.9 l/min Ar
Rf power	1550 W
Backgrounds	
ThO/Th ratio (cps) of NIST610	<0.5%
Dwell time per isotope	10 ms, except 20 ms: ^{32}S, 40 ms: ^{35}Cl, 60-80 ms: ^{79}Br

Chlorine concentrations in NIST610 are low and not well characterized. In-house characterized natural scapolite Sca17 was used as SRM for Cl and Br analysis. Chlorine concentration in Sca17 (2.9 ± 0.2 wt%) and AfgAA (4.1 ± 0.3 wt%) were determined by EPMA. For EPMA Cl quantifications of Sca17 and AfgAA by EPMA, we used stoichiometries of pure halite (ETHZ), tugtupite (UTAS; $Na_4AlBeSi_4O_{12}Cl$), and vanadinite (Bayreuth; $Pb_5V_3O_{12}Cl$) as external SRM. Br concentrations in Sca17 (438 ± 22 □g/g) and NIST610 (33 ± 4 □g/g) were determined by using a synthetic Br-bearing silicate glass for calibration and LA-ICP-MS. The Br-concentration (0.96 ± 0.04 wt%) of the synthetic glass was measured by Rutherford Backscattered Spectroscopy (RBS). Homogeneities of the Cl (0.6 % RSD) and Br

(5.0 %) in Sca17 were checked by repeated LA-ICP-MS spot measurements. Concentrations in the standard reference materials are reported in Table 2.

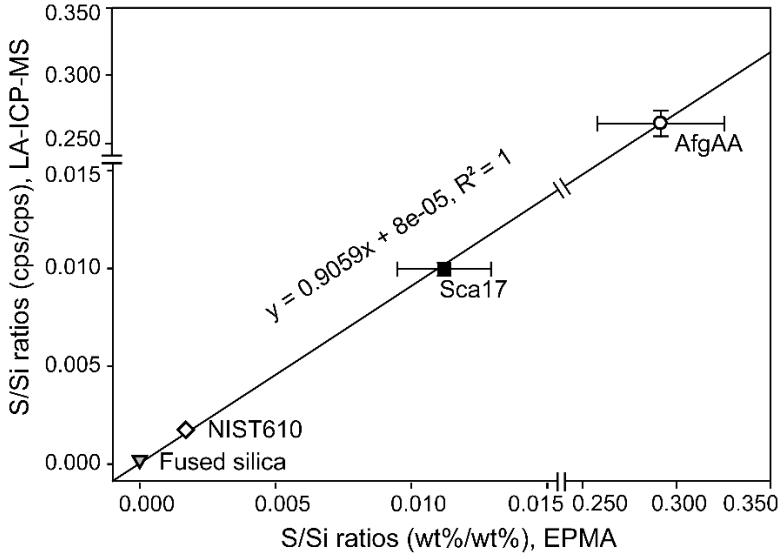

Figure 1. Calibration curve of sulfur/silicon cps ratios by LA-ICP-MS and independently analyzed or reported wt% ratios in NIST610 glass, Sca17 and AfgAA, showing good correlation. The relatively large error on the S/Si ratio on Sca17 and AfgAA in the EPMA value includes the variation due to different sulfur calibration strategies in 3 different laboratories.

Table 2. Sulfur, chlorine, bromine concentrations in NIST610, Sca17 (scapolite), and AfgAA (afghanite) standards used as external standards for fluid inclusion analyses. Sulfur and chlorine concentrations in the Sca17 and AfgAA standards are measured by electron-probe micro-analysis (EPMA) at ETH Zurich, University of Tasmania, and University of Bayreuth. Br concentrations in the NIST610 and Sca17 standards are measured by LA-ICP-MS with Br-bearing silicate glass external standard. Br concentration in the silicate glass is determined by Rutherford Backscattered Spectroscopy (RBS).

	NIST SRM 610 (µg/g)	Sca17 (µg/g)	AfgAA (µg/g)
Sulfur	550 ± 40 (LA-ICP-MS)*	2,900 ± 470 (EPMA)**	43,000 ± 4,690 (EPMA)**
Chlorine	not determined	28,900 ± 1,960 (EPMA)**	40,800 ± 2,740 (EPMA)**
Bromine	33 ± 4 (LA-ICP-MS)***	438 ± 22 (LA-ICP-MS)***	not determined

* Guillong et al. (2009)

** EPMA results from ETH Zurich, University of Tasmania, and University of Bayreuth

*** Calibrated with Br-bearing glass measure with RBS

Element concentrations, uncertainties, limits of detection (LOD), and element ratios of single fluid inclusions were calculated from transient fluid inclusion signals applying the SILLS software (Guillong et al., 2008b) that uses the deconvolution of host and inclusions signals described by Halter et al. (2002) and Heinrich et al. (2003). Element ratios measured by LA-ICP-MS with the external standardizations by NIST610 and Sca17 were converted into absolute concentrations by using internal standards. We used Cs as an internal standard for sulfur analysis with NIST610 as external standard, and Sca17 as external standard to determine Br/Cl ratios. For absolute Br and Cl quantification, we used Na as internal

standard because its concentration in Sca17 is well characterized.

Results are reported by averaging the concentrations or element ratios of all analyses of n single fluid inclusions in one assemblage (n = 4-11). Calculation of uncertainties, including individual measurements and the variation among an assemblage, are discussed below.

2.3. Synthetic Fluid Inclusions

We synthesized liquid and vapor inclusions with variable S, Cl and Br concentrations to check the accuracies and precisions of the S, Cl, and Br analysis by LA-ICP-MS microanalysis. Three liquid inclusion samples were produced in a piston cylinder apparatus at ETH Zurich. Solutions were made from ultra pure water, NaCl, Na_2SO_4*10(H_2O), NaBr, CsCl and loaded into Ag or Cu capsules containing pre-fractured quartz. 10 kbar and 600°C were applied for 6-7 days. Three quartz chips with synthetic vapor inclusions were prepared at the University of Maryland, in a rapid-quench titanium zirconium molybdenum (TZM) pressure vessel using Ar-H_2 as pressure medium. Experimental runs contained ultra pure water, elemental S, NaCl, NaBr, CsCl, and RbCl. The S was reduced to H_2S during the 50-60 hours run with 1.6-1.7 kbar of pressure and 950-1000°C of temperature. Concentrations of the starting solutions are listed in Table 2. Densities of the entrapped fluids are calculated based on the applied pressure and temperature and prepared chloride contents (Driesner and Heinrich, 2007) (Table 3).

Table 3. Details of experimental conditions used for the synthesis of fluid inclusions containing standard solutions.

	JH#1 (liq.)	JH#2 (liq.)	JH#3 (liq.)	ZZ#1 (vap.)	ZZ#86 (vap.)	ZZ#88 (vap.)
Cl (µg/g)	47,784	3,645	19,532	16,602		
Na (µg/g)	37,015	48,893	39,904	10,767	11,520	10,329
Br (µg/g)	139	180	230	93		
Rb (µg/g)				183	191	177
Cs (µg/g)	832	655	847	183	190	176
S (µg/g)	4,299	32,514	19,071	40,804	24,500	100,900
Cl/Br (atomic ratio)	344	20	85	179		
Densities of fluids (g/cm^3)	1.02	0.99	1.00	0.33	0.33	0.33
Total dissolved solids (wt%)	9.0	8.6	8.0	6.9	3.6	11.0
	10 kbar, 600 ℃, 6-7 days, ETH Zurich			1.6-1.7 kbar, 950-1000 ℃, 51-62 hours, University of Maryland		
	Piston cylinder, Ag or Cu capsules			TZM pressure vessel, Cu-Au capsules		

3. **Results and discussions**

3.1. Source of Sulfur Contamination and Cleaning of the Ablation Chamber

Internal contamination causes elevated S, and lesser Cl and Br signals above gas blank levels, even during ablation of the host quartz alone (Figure 2). Here we report our cleaning procedure to minimise this contamination. For analyzing the concentration of an element in quartz-hosted fluid inclusions, we require the count ratio of element/Si to subtract any contribution of the host mineral to the inclusion signal, by assuming a negligible amount of Si dissolved in the fluid at trapping conditions. Severe increases of S signals corresponding to a S/Si cps ratio of ~ 0.01 are observed during the ablation of pure quartz, corresponding to an apparent S concentrations in quartz around 200 μg/g. Cl and Br signals show a similar but less significant increase during pure quartz ablation (cps ratio of Cl/Si and Br/Si are 0.00023 and 0.00003, respectively). We showed previously that there is no sulfur in the quartz itself (Guillong et al., 2008a). However, the sulfur contamination severely limits the detection of sulfur in the fluid inclusions, because the spurious S/Si ratio is not constant through time, making subtraction difficult and uncertain. Figure 2 illustrates how the S contamination gradually decreased from 0.010 to 0.008 over the time of a typical measurement block, in response to repeated quartz ablations with 100 μm crater diameter. If pure silica is ablated close to a grain of elemental sulfur or a sulfur-bearing rubber O-ring inside the ablation chamber, the sulfur intensity increases significantly, even without any direct ablation of the sulfur-bearing materials (Figure 3). The radiations of 193 nm UV laser or possibly the laser induced plasma mobilize sulfur from surfaces in the interior of the ablation chamber. We also found enhanced sulfur background while irradiating the empty chamber with a defocused UV laser (Figure 2), showing that direct or indirect UV radiation mobilizes sulfur contamination from inside the ablation chamber and increases the background level of sulfur. Therefore, we carefully cleaned all inside parts of the ablation chamber that are exposed to UV light, first by rubbing the inside of the ablation chamber with detergent for metal materials, followed by soaking the body of the ablation chamber in concentrated nitric acid. After this cleaning procedure, we found significantly reduced sulfur contamination (Figure 3) during ablation of quartz. After additional "UV cleaning" ablations with 100 μm crater diameters on quartz, the S/Si cps ratio went down to 0.002, and the apparent sulfur concentrations in quartz were reduced about 10 fold. The S/Si ratio did not increase again after ablating SRMs and the sulfur-bearing rubber O-ring, nor after opening and closing the ablation chamber several times during a day (Figure 3). Over several days however, the S contamination slowly increased again, but we are not sure whether S is accumulating on the surfaces from the ablation of the weakly S-bearing samples or from a sulfur impurity of the $He+H_2$ gas.

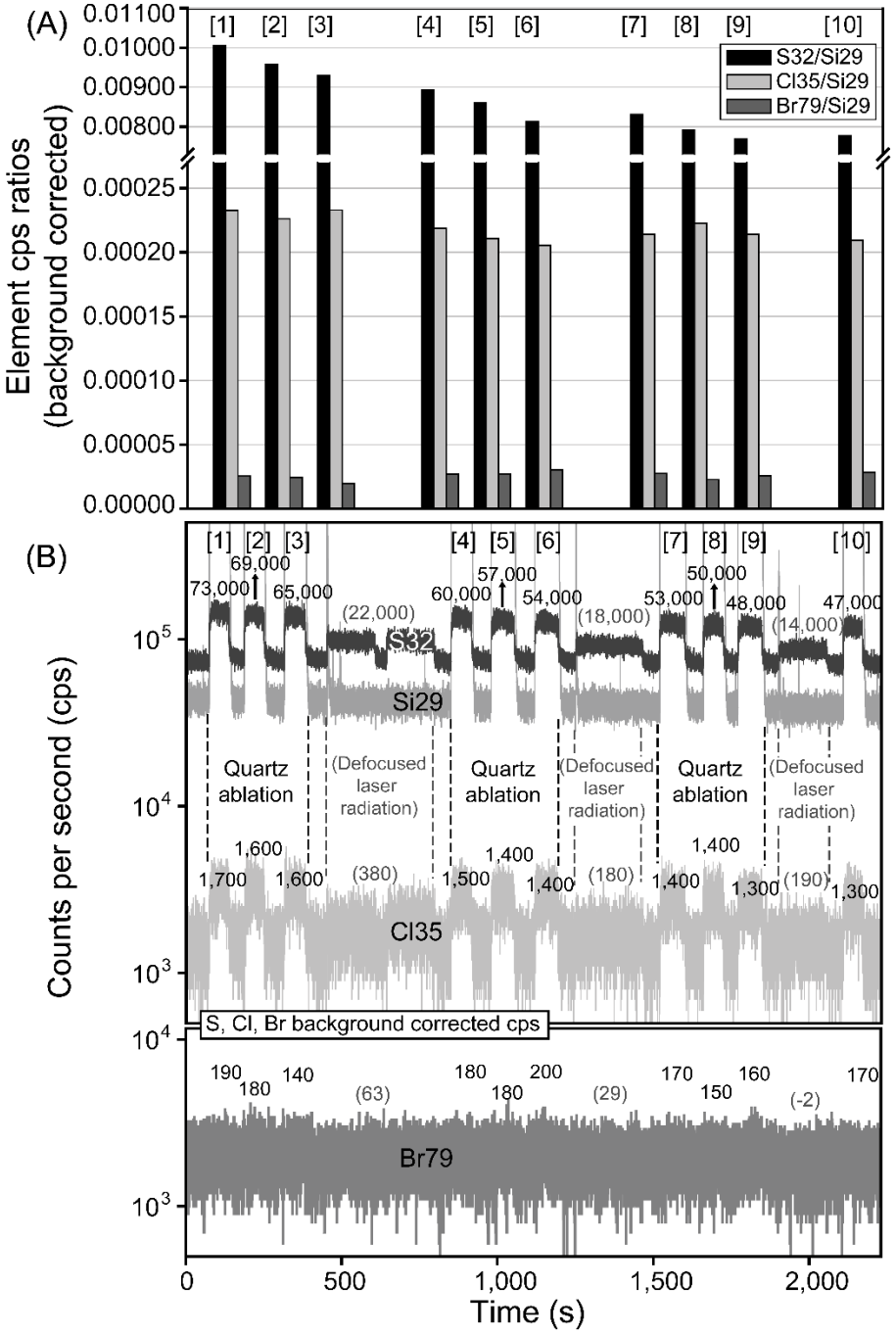

Figure 2. Element/Si cps ratios (**A**) and gas-blank-corrected transient S, Cl, and Br signals (**B**) of quartz ablations and defocused UV laser radiation before cleaning of the ablation chamber showing high initial S contamination levels (S/Si of 0.01, Cl/Si of 0.0002, and Br/Si of 0.00002). After the repeated laser ablations of the quartz with 10 Hz and 100 μm crater diameter and defocused laser irradiations, S/Si level decreased to 0.008, while Cl/Si, Br/Si cps ratios remain similar. Each column represents background-corrected element/Si cps ratios of individual quartz ablation.

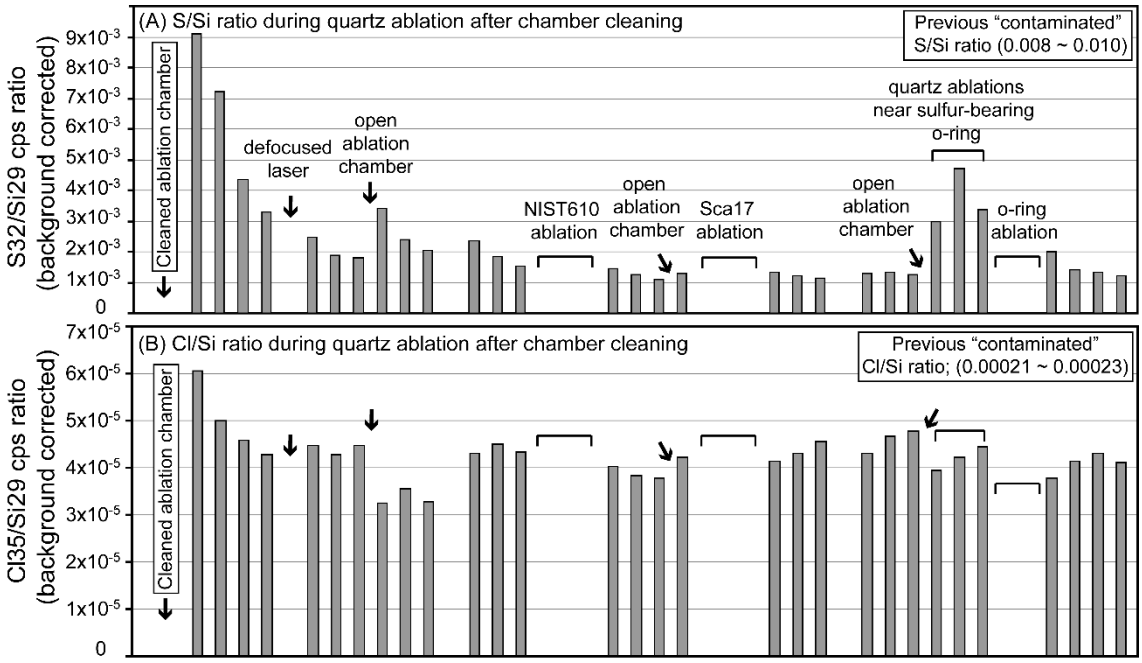

Figure 3. The variation of S/Si and Cl/Si signals in response to the cleaning of the ablation chamber. Each column represents background-corrected element/Si cps ratios of individual quartz ablation in a time sequence from left to right, in a single analysis session without instrumental re-tuning. After the cleaning of the ablation chamber and several laser ablations on quartz, S/Si cps ratio went down to 0.002 and Cl/Si cps ratios went down to 0.00006. S/Si ratios do not change much after opening and closing the ablation chamber, ablations of S-bearing standard reference materials (Sca17 and NIST610), and ablations of S-bearing rubber o-ring.

With cleaning of the ablation chamber every few days, we now routinely reach S/Si cps ratio approximately 0.004 above gas blank, making the baseline correction of quartz hosted fluid inclusions easier (Figure 4) compared to our previous analyses (Guillong et al., 2008a). Detection limit for sulfur of 30 µm sized brine inclusion around 100 µg/g is significantly reduced from around 300 µg/g obtained from similar inclusions prior to cleaning of the ablation cell (Seo in Ripley et al., in press). Cl/Si and Br/Si ratios during quartz ablations were also lowered somewhat to between 0.000035 and 0.00001 (initial Cl/Si and Br/Si are from 0.00023 and 0.00003), respectively, improving the LOD on chlorine and bromine (Figure 4). Since we cannot completely remove the S contamination, we still have to carefully define baselines of host S/Si signals and host correction intervals for correct quantification of total sulfur counts of the inclusion (Guillong et al., 2008a) (Figure 4).

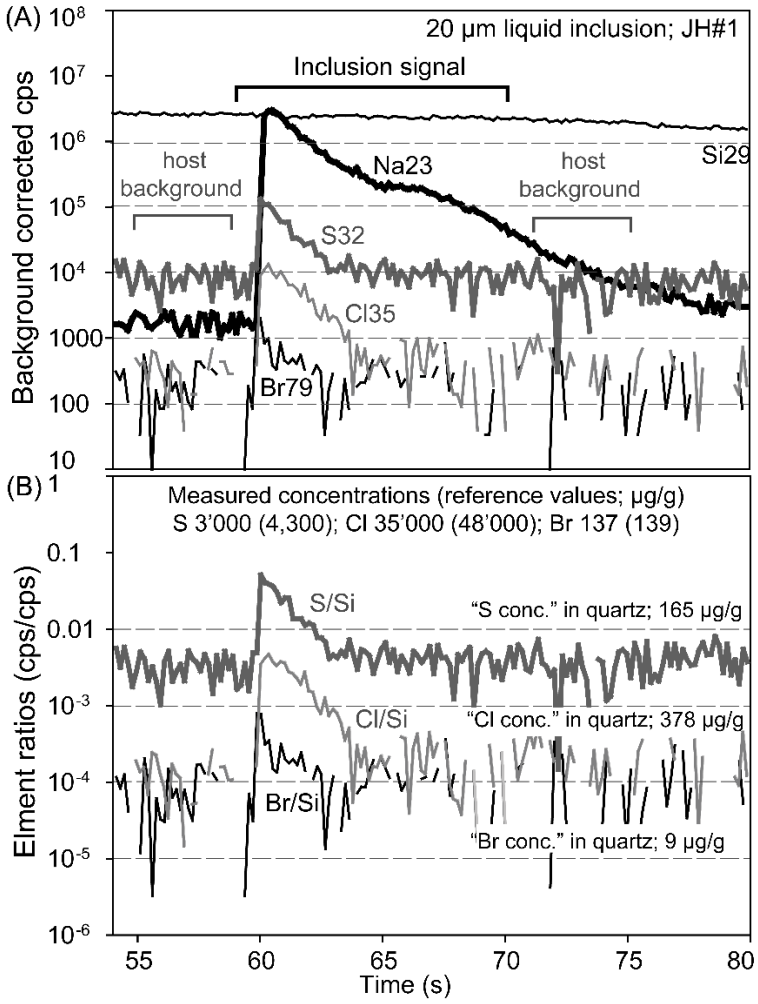

Figure 4. (**A**) Background corrected transient signal of synthetic fluid inclusion (**B**) Element/Si cps ratios of S, Cl, and Br with apparent (contaminated) concentrations of the elements in quartz.

3.2. Accuracy and Precision

LA-ICP-MS analyses of synthetic fluid inclusions produce good accuracy of S concentration and Br/Cl ratios with reasonable precision of S (16-45% error) and Br/Cl atomic ratio (5-25% error) based on the variation of several individual fluid inclusions in an assemblage (Figure 5, 6 and Table 4, 5). The reproducibility of the concentrations for Cl between 7-20% and for Br between 12-26% (Table 5) might indicate that the uncertainly of Br is the main source of uncertainty for Br/Cl ratio (5-25%), because the signal for Br that is closer to the detection limit than for the more concentrated Cl in the fluid inclusions. However, the uncertainty of the Br/Cl ratio is smaller than the uncertainties of individual Cl and Br concentrations. We therefore attribute the additional uncertainty in absolute concentration to the uncertainty from internal standardization (Na content). In fact, we found that the Br concentrations calculated by Na internal standard are less accurate and precise than by

taking Cl as internal standard (Table 5). Detections of Br and Cl in synthetic vapor inclusions were not possible due to their low density and low concentration.

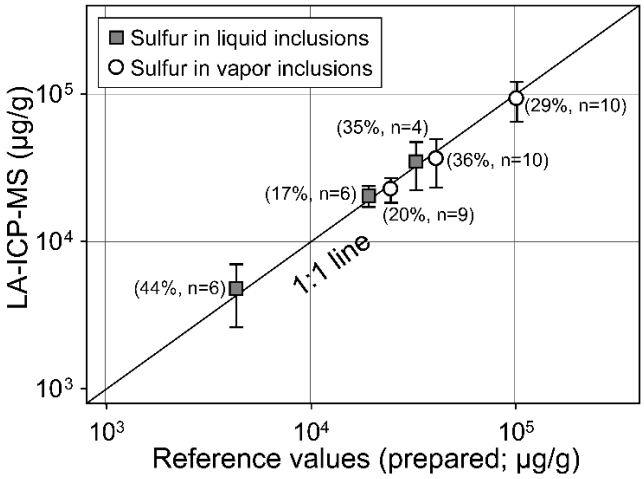

Figure 5. Accuracies and precisions of sulfur analysis in synthetic liquid and vapor inclusions. Errors (%) and numbers (*n*) in the brackets represent % of 1σ/average and number of single analysis of the assemblages, respectively.

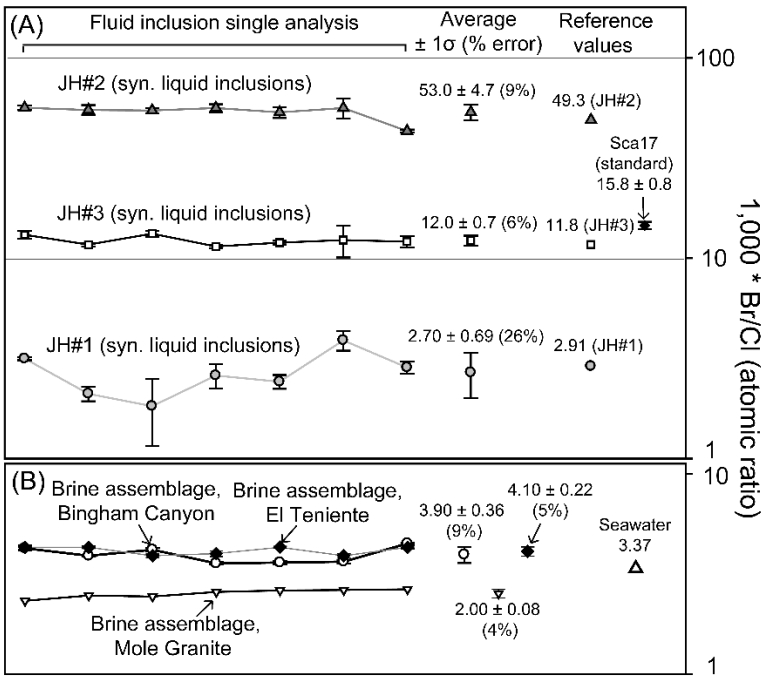

Figure 6. 1000*Br/Cl atomic ratios of (**A**) synthetic and (**B**) natural fluid inclusion single analysis, average and error (±1σ) of an assemblage of 7 cogenetic inclusions in each sample with comparative reference values. Accuracies and precisions of the Br/Cl ratios of in three samples of synthetic fluid inclusions (A; JH#1, JH#2, and JH#3) are compared with the prepared reference composition and the external scapolite mineral standard (Sca17) , (B) Three natural brine inclusion assemblages from the Bingham Canyon (9 % error) and El Teniente porphyry copper deposits (5 % RSD), and the Sn-W-mineralized Mole Granite (4 % RSD).

Table 4. Results of sulfur analyses of synthetic fluid inclusions with the reference values. NIST610 and Cs were used as external and internal standard, respectively, for the quantification of S in fluid inclusions.

	Inclusion size(μm)	Inclusion mass (μg)	Na (μg/g)	S (μg/g)	LOD of S	Error of S (1 σ)	*Cs (μg/g)	Rb (μg/g)
JH#1 (Reference)			**37,015**	**4,299**			**832**	
09nv11a06	20	0.0043	35,000	2,900	100	95	832	
09nv11a08	15	0.0018	75,000	4,900	230	200	832	
09nv11a09	20	0.0043	68,000	5,600	270	200	832	
09nv11a10	15	0.0018	62,000	7,400	610	420	832	
09nv11a11	15	0.0018	55,000	6,200	850	560	832	
09nv11a13	30	0.0144	39,000	1,500	75	49	832	
Average			**55,000**	**4,800**				
1 σ (RSD)			**15,000 (27%)**	**2,100 (44%)**				
JH#2 (Reference)			**48,893**	**32,514**			**655**	
09nv10b06	20	0.0041	45,000	26,000	190	170	655	
09nv10b07	25	0.0081	39,000	25,000	96	110	655	
09nv10b08	25	0.0081	81,000	52,000	410	350	655	
09nv10b09	25	0.0081	52,000	35,000	160	130	655	
Average			**54,000**	**34,000**				
1 σ (RSD)			**18,000 (33%)**	**12,000 (35%)**				
JH#3 (Reference)			**39,904**	**19,071**			**847**	
09nv10b11	25	0.0082	41,000	20,000	260	410	847	
09nv10b12	25	0.0082	48,000	18,000	100	150	847	
09nv10b13	30	0.0141	62,000	22,000	57	61	847	
09nv10b14	25	0.0082	61,000	19,000	140	110	847	
09nv10b15	25	0.0082	66,000	25,000	150	130	847	
09nv10b17	20	0.0042	46,000	16,000	260	240	847	
Average			**54,000**	**20,000**				
1 σ (RSD)			**10,000 (19%)**	**3,300 (17%)**				
ZZ#1 (Reference)			**10,767**	**40,804**			**183**	**183**
09nv10c06	25	0.0027	11,000	34,000	670	780	183	180
09nv10c07	15	0.0006	11,000	43,000	1,600	1,300	183	190
09nv10c08	20	0.0014	12,000	57,000	2,600	2,500	183	170
09nv10c09	20	0.0014	13,000	27,000	2,200	2,900	183	180
09nv10c09c	30	0.0046	11,000	20,000	260	330	183	160
09nv10c10	20	0.0014	10,000	31,000	1,100	1,500	183	190
09nv10c11	20	0.0014	12,000	47,000	400	490	183	180
09nv10c12	15	0.0006	12,000	34,000	1,800	1,900	183	170
09nv10c13	20	0.0014	12,000	16,000	2,400	3,100	183	190
09nv10c15	20	0.0014	11,000	49,000	1,200	930	183	180
Average			**11,000**	**36,000**				**180**
1 σ (RSD)			**790 (7%)**	**13,000 (36%)**				**7 (4%)**
ZZ#86 (Reference)			**11,520**	**24,500**			**190**	**191**
09nv15b03	20	0.0014	10,000	22,000	1,100	1,000	190	200
09nv15b04	25	0.0027	11,000	21,000	740	660	190	220
09nv15b05	25	0.0027	11,000	21,000	720	740	190	200
09nv15b06	20	0.0014	11,000	19,000	1,500	1,700	190	210
09nv15b07	20	0.0014	16,000	29,000	1,600	1,700	190	200
09nv15b09	25	0.0027	10,000	18,000	780	1,300	190	190
09nv15b11	20	0.0014	10,000	17,000	1,500	1,800	190	180
09nv15b12	20	0.0014	11,000	23,000	1,300	1,600	190	220
09nv15b13	25	0.0027	11,000	29,000	1,600	1,600	190	210
Average			**11,000**	**22,000**				**200**
1 σ (RSD)			**1,700 (15%)**	**4,300 (20%)**				**12 (6%)**
ZZ#88 (Reference)				**100,900**			**176**	**177**
09nv15c03	15	0.0006		82,000	1,700	2,000	176	180
09nv15c04	20	0.0014		73,000	1,400	1,600	176	200
09nv15c05	20	0.0014		150,000	3,300	3,800	176	180
09nv15c06	20	0.0014		75,000	2,100	2,100	176	160
09nv15c07	30	0.0046		110,000	1,800	1,700	176	180
09nv15c08	20	0.0014		77,000	3,900	3,800	176	180
09nv15c09	30	0.0046		77,000	760	1,100	176	160
09nv15c10	30	0.0046		77,000	2,600	3,000	176	210
09nv15c11	15	0.0006		73,000	2,500	3,500	176	160
09nv15c13	20	0.0014		110,000	2,900	3,100	176	220
Average				**92,000**				**180**
1 σ (RSD)				**27,000 (29%)**				**21 (12%)**

* Cs Internal standard with NIST610 glass external standard

In addition to variations between cogenetic inclusions, we also calculated uncertainty contributions from the transient signals of single fluid inclusions using SILLS (Guillong et al., 2008b). The methodology of the uncertainty and LOD calculation was developed by Halter et al. (2002) and considers two factors, counting statistics and noise in the ICP signal. The uncertainty due to counting statistics is based on total counts of a certain element integrated over the time period of the transient inclusion signal. The uncertainty from the noise in the ICP signals, mainly due to the inherent instability of the plasma ion source, can be calculated from the standard deviation of the gas background in the transient signals. Applying longer dwell times for an element reduces the variability of the recording backgrounds (Guillong et al., 2008b; Halter et al., 2004). Systematic errors, however, can be generated by incomplete recording of short transient signals with multi-element menus (Pettke et al., 2000), which cannot be evaluated from the transient signal. Figure 7 indicates that statistical uncertainties of single analysis of synthetic fluid inclusions, with the exception of some of the weakest Br signals close to detection, is small compared to variations among multiple inclusion measurements in a fluid inclusion assemblages. The latter is probably dominated by the uncertainty from incomplete recording of the irregular transient signals, because there is no reason to assume real compositional variation. Therefore, to get reliable fluid inclusion compositions, we recommend analyzing many fluid inclusions belonging to one fluid inclusion assemblage assumed to be compositionally homogeneous and using the average values along with their standard deviation.

3.3. Limits of Detection (LOD)

LOD for elements in fluid inclusions mainly depends on sensitivities of the LA-ICP-MS instrument, the size and densities of the FI, and is also influenced by the sharpness of the transient signal (e.g. height of fluid inclusion signal above background). We calculated the mass of each fluid inclusions from estimated fluid densities (by the entrapment P-T and starting compositions) and inclusion volumes, based on the average diameter and assuming spherical shape. The limit of detection is inversely correlated with the mass of the inclusion (Figure 8, 9). The respective detection limits of S, Cl, and Br of 25-35 μm sized liquid inclusion are ~ 160 μg/g (n=9), 340 μg/g (n=7), and 17 μg/g (n=7). The LOD of S of fluid inclusions after cleaning of ablation chamber are about 2 times better than the previously reported values (Guillong et al., 2008a), due to the lower S background during quartz ablation.

Table 5. Analyzed chlorine and bromine concentrations in synthetic liquid inclusions with the reference values. Scapolite mineral (Sca17) and Na were used as external and internal standard, respectively, for chlorine and bromine quantifications.

	Inclusion size (µm)	Inclusions mass (µg)	*Na (µg/g)	*Cl (µg/g)	1σ of Cl (% RSD)	LOD of Cl	*Br (µg/g)	1σ of Br (% RSD)	LOD of Br	**Br (µg/g ± 1σ)	1000·(Br/Cl) (atomic ratio)	1σ of 1000·Br/Cl (% RSD)
JH#1 (Reference)			**37,015**	**47,784**			**139**			**139**	**2.91**	
10ma20c05	70	0.1834	37,015	46,000	160 (0.3%)	40	140	2 (1.5%)	3	150 ± 2	3.10	0.06 (1.9%)
10ma20c06	40	0.0342	37,015	53,000	370 (0.7%)	121	110	8 (7.6%)	8	99 ± 9	2.10	0.17 (8.3%)
10ma20c08	60	0.1155	37,015	52,000	840 (1.6%)	898	97	35 (35.7%)	54	89 ± 35	1.80	0.67 (37.3%)
10ma20c10	30	0.0144	37,015	46,000	520 (1.1%)	335	120	15 (12.6%)	19	120 ± 15	2.60	0.36 (13.8%)
10ma20c11	50	0.0668	37,015	49,000	350 (0.7%)	184	120	9 (7.3%)	10	120 ± 9	2.40	0.19 (8.0%)
10ma20c12	25	0.0084	37,015	52,000	650 (1.2%)	424	200	20 (10.0%)	23	180 ± 21	3.90	0.44 (11.2%)
10ma20c14	50	0.0668	37,015	45,000	270 (0.6%)	157	130	9 (6.7%)	8	140 ± 9	2.80	0.20 (7.3%)
Average			**37,015**	**49,000**			**130**			**130**	**2.70**	
1 σ (RSD)				**3,500 (7%)**			**35 (27%)**			**32 (26%)**	**0.69 (26%)**	
JH#2 (Reference)			**48,893**	**3,645**			**180**			**180**	**49.26**	
10ma20a04	45	0.0472	48,893	4,100	63 (1.5%)	40	230	3 (1.2%)	2	200 ± 3	56.00	1.50 (2.7%)
10ma20a05	35	0.0222	48,893	4,200	140 (3.2%)	295	230	6 (2.5%)	14	200 ± 6	55.00	3.20 (5.8%)
10ma20a07	40	0.0331	48,893	4,100	71 (1.7%)	50	220	3 (1.3%)	2	200 ± 3	54.00	1.66 (3.1%)
10ma20a09	35	0.0222	48,893	4,700	120 (2.6%)	271	260	5 (2.0%)	13	200 ± 5	56.00	2.60 (4.6%)
10ma20a11	50	0.0647	48,893	4,000	140 (3.5%)	222	210	6 (2.8%)	10	190 ± 6	53.00	3.40 (6.3%)
10ma20a12	35	0.0222	48,893	3,800	240 (6.4%)	778	210	11 (5.1%)	36	200 ± 11	56.00	6.50 (12.0%)
10ma20a13	70	0.1776	48,893	4,100	38 (0.9%)	25	170	1 (0.8%)	1	150 ± 1	43.00	0.76 (1.8%)
Average			**48,893**	**4,100**			**220**			**190**	**53.00**	
1 σ (RSD)				**280 (7%)**			**26 (12%)**			**19 (9%)**	**4.70 (9%)**	
JH#3 (Reference)			**39,904**	**19,532**			**230**			**230**	**11.78**	
10ma20b03	40	0.0335	39,904	17,000	210 (1.2%)	187	230	8 (3.3%)	9	260 ± 8	13.00	0.60 (4.6%)
10ma20b04	35	0.0225	39,904	21,000	140 (0.6%)	51	240	3 (1.4%)	3	220 ± 3	11.00	0.22 (2.0%)
10ma20b05	40	0.0335	39,904	16,000	160 (1.0%)	106	220	5 (2.4%)	5	270 ± 5	13.00	0.45 (3.4%)
10ma20b06	75	0.2210	39,904	21,000	130 (0.6%)	40	240	3 (1.3%)	2	220 ± 3	11.00	0.21 (1.9%)
10ma20b07	60	0.1132	39,904	19,000	130 (0.7%)	45	230	3 (1.5%)	2	240 ± 3	12.00	0.26 (2.2%)
10ma20b08	50	0.0655	39,904	12,000	490 (4.1%)	488	150	22 (14.6%)	26	240 ± 23	12.00	2.20 (18.7%)
10ma20b12	30	0.0141	39,904	24,000	400 (1.6%)	249	290	14 (4.9%)	15	240 ± 15	12.00	0.79 (6.6%)
Average			**39,904**	**19,000**			**230**			**240**	**12.00**	
1 σ (RSD)				**3,800 (20%)**			**42 (18%)**			**18 (6%)**	**0.68 (6%)**	

* Na Internal standard with Sca17 external standard

** Cl internal standard with Sca17 external standard

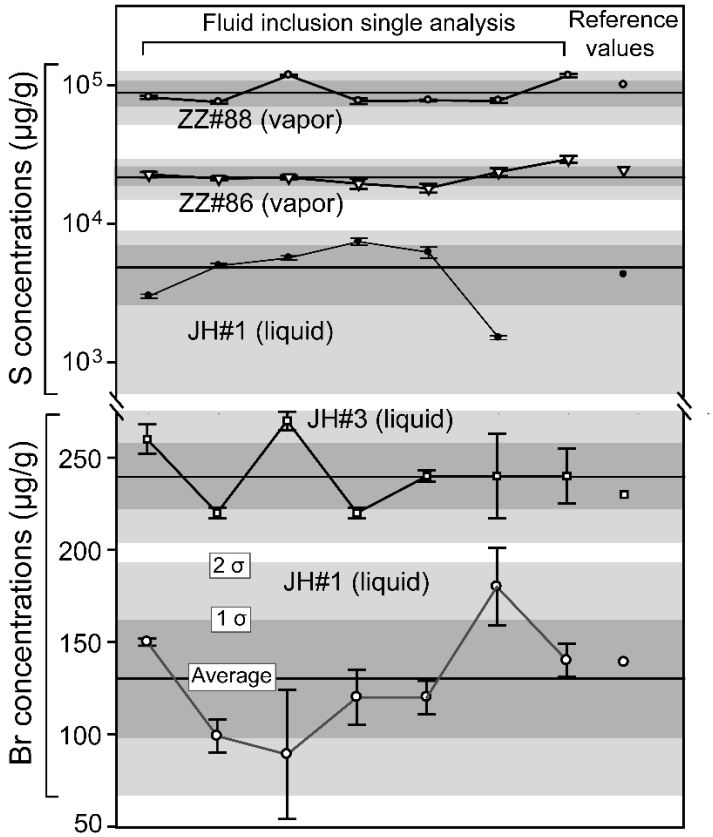

Figure 7. Averages (centerline) and errors (shades; ±1σ and ±2σ) of the S and Br analyses in the synthetic fluid inclusion assemblages are plotted with errors of the individual fluid inclusion analysis calculated from counting statistics alone. Note that the S and Br fluid inclusion analyses are conducted separately. Absolute S and Br concentrations are calculated using Cs and Cl internal standards, respectively. Note that S values are plotted in log scale and Br values are plotted in linear scale.

3.4. Sulfur and Bromine/Chlorine ratios of Natural Fluid Inclusions

In this section, we apply sulfur and precise Br/Cl ratio of analyses to natural fluid inclusions. Sulfur and cations are calibrated with NIST610 glass external standard. Ratios of chlorine and bromine are calibrated with Sca17 as external standard. Salinity corrections and internal standardizations to obtain absolute concentrations were carried out following the method of Heinrich et al. (2003). For the analyses of Br/Cl ratios in natural fluid inclusion, we increased the quality of Br and Cl determination by a reduced element set including only Na, Si, Cl and Br, which are homogeneously distributed in the Sca17 standard.

We measured sulfur and important cations such as K, Fe, Cu, Zn, As, Ag, Cs, Pb, and Au in a natural assemblage of vapor inclusions with a bulk density of about 0.33 g/cm^3 estimated from the microthermometrically measured vapor salinity and the estimated trapping temperature from cogenetic brine-vapor assemblage (boiling assemblage) nearby. The free-standing quartz crystal was sampled from a miarolitic cavity from the Chernomorets quartz

monzonite (Bulgaria). The analyzed 11 vapor inclusions contained 6'200 µg/g of sulfur and the 1 RSD error (percent of 1σ/average) of sulfur analyses was 27% (Figure 8). While simultaneously detecting the trace metals such as Ag and Au with respective dwell times of 20 ms and 50 ms, we obtained sulfur LOD of 200 µg/g for 35 µm sized natural vapor inclusions (Figure 8). The LOD of S in the low density vapor inclusion is comparable to the one we previously obtained from 35 µm sized high-density brine inclusions, and the standard deviation within the vapor assemblage is even improved slightly (Guillong et al., 2008a).

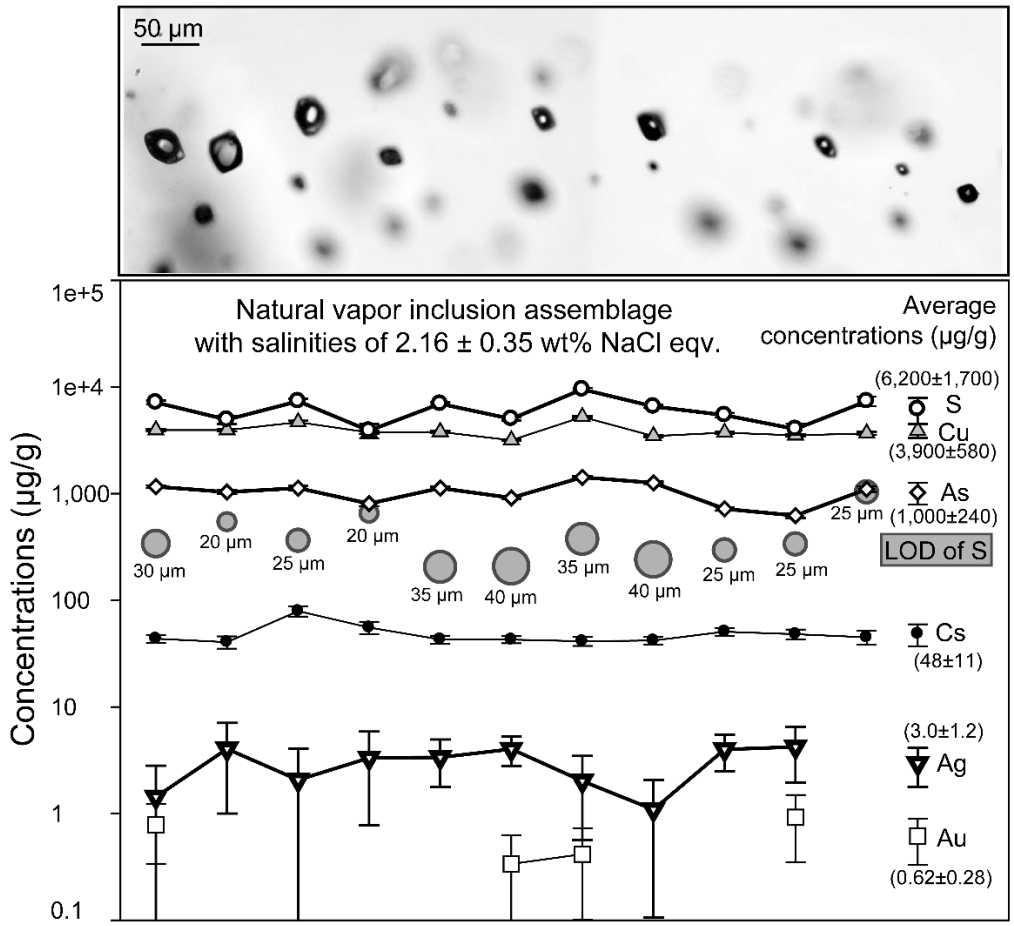

Figure 8. Concentrations of selected elements from a natural vapor inclusion assemblage in a miarolitc quartz crystal (Chernomoretz quartz monzonite intrusion, Bulgaria). Size of the inclusions and individual limits of detection for sulfur are negatively correlated.

We measured Br and Cl, and calculated the precisions of Br/Cl ratios of natural high density brine inclusion assemblages hosted in quartz veins from three magmatic-hydrothermal ore systems: the Mole Granite, Australia (Sn-W deposit), El Teniente, Chile (Cu-Mo deposit) and Bingham Canyon, USA (Cu-Mo-Au deposit) (Figure 6 and Table 7). The 1000*(Br/Cl) atomic ratios in the brine inclusion assemblages from Mole Granite, El Teniente, and Bingham

Canyon are 2.00 ± 0.08 (4% relative error), 4.10 ± 0.22 (5% error), and 3.90 ± 0.36 (9% error), respectively. Due to its high salinities (35-40 wt% NaCl equiv.) overall high concentrations of Cl and Br, and the big size of the natural inclusions (generally larger than 30 μm diameter), uncertainties for these brine inclusions assemblages are much smaller than those of synthetic fluid inclusion assemblages. The analyses show that the precisions of the Br/Cl ratios in the natural fluid inclusion assemblages measured by LA-ICP-MS are good enough to distinguish the ratios of the fluids in different magmatic-hydrothermal deposits. The high Br solubility in silicate melt and similar solubility of Cl and Br in various melt composition (Bureau and Metrich, 2003) makes the Br/Cl ratio of magmas sensitive to the incorporation of an NaCl-enriched source such as seawater and evaporites. The Br/Cl ratios in the brines of the two porphyry copper deposits are similar and close to seawater composition, consistent with their association with recent (Skewes et al., 2002) and possibly ancient subduction (Bingham Caynon) (Pettke et al., 2010). By contrast, the fluids from the crustal-derived Mole Granite (Sn-W deposit) have Br/Cl distinctly below modern seawater (Figure 6), which might indicate that the Mole Granite has incorporated Cl-enriched evaporitic sedimentary rocks. Many other processes could play a role to fractionate Br/Cl ratios in the fluids, such as preferential melt-fluid partitioning (Villemant and Boudon, 1999), magma fractionation (Balcone-Boissard et al., 2010; Villemant and Boudon, 1999), and fluid phase separation (Liebscher et al., 2006). The new ability for texturally controlled fluid inclusion analysis offers a new road to exploring these alternative processes.

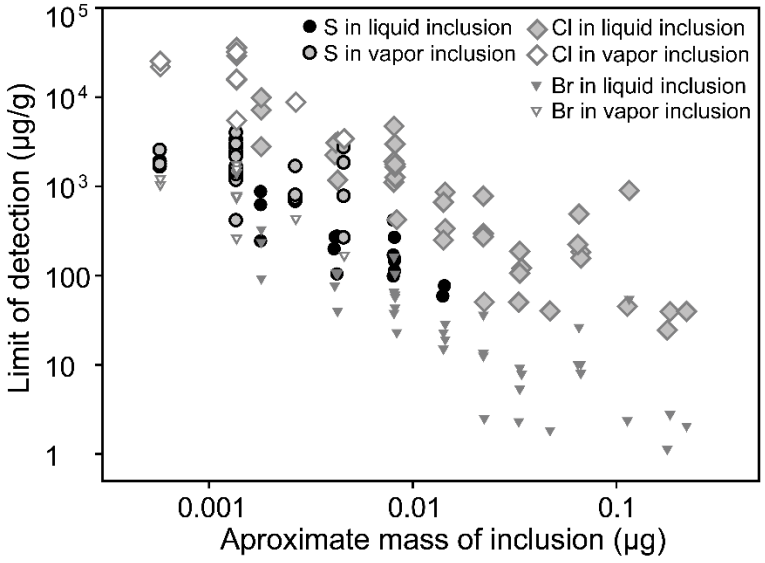

Figure 9. Inverse correlations between detection limits (μg/g) of S, Cl, and Br analyses in synthetic fluid inclusions by LA-ICP-MS versus mass of the inclusions (μg). The mass of the inclusions are calculated using the estimated densities (Driesner and Heinrich, 2007) of the synthesized fluids and volumes of fluid inclusions. The volumes of the inclusions are estimated by the FI diameters and assumption of spherical FI shape.

Table 6. Concentrations of sulfur and some cations in a natural low-salinity vapor inclusion assemblage (2.16 ± 0.35 wt% NaCl eqv.) from a miarolitic quartz crystal (Chernomoretz quartz monzonite intrusion, Bulgaria). Errors and limits of detections for sulfur are reported for each individual analysis.

	Inclusion size (μm)	Na (μg/g)	S (μg/g)	error of S (1σ)	LOD of S	K (μg/g)	Fe (μg/g)	Cu (μg/g)	Zn (μg/g)	As (μg/g)	Ag (μg/g)	Cs (μg/g)	Au (μg/g)	Pb (μg/g)
Vapor-rich assemblage, Free-standing quartz in miarolitic cavity, Chernomeretz quartz monzonite intrusion														
10fe03a03	30	6,500	7,200	290	330	2,200	1,700	3,900	270	1,200	1.4	44	0.78	140
10fe03a04	20	6,800	4,900	460	530	<540	1,900	3,900	160	1,000	4.0	41	<0.44	120
10fe03a05	25	6,500	7,300	430	350	2,200	840	4,700	290	1,100	2.1	79	<0.37	170
10fe03a06	20	6,500	3,900	600	630	2,400	2,300	3,700	230	810	3.3	56	<0.80	150
10fe03a07	35	7,100	6,900	240	200	<200	830	3,800	230	1,100	3.4	43	<0.14	110
10fe03a08	40	6,700	5,000	190	200	1,700	1,100	3,200	230	910	4.0	43	0.34	130
10fe03a09	35	6,800	9,500	330	360	1,800	1,700	5,200	190	1,400	2.0	41	0.42	130
10fe03a10	40	6,700	6,600	240	230	1,800	830	3,500	160	1,300	1.1	42	<0.20	100
10fe03a11	25	7,300	5,400	270	290	<290	1,700	3,700	200	720	4.0	51	<0.21	120
10fe03a13	25	6,600	4,000	480	320	2,000	1,700	3,500	180	620	4.2	48	0.92	120
10fe03a15	25	6,600	7,400	740	1,000	1,800	1,200	3,700	330	1,100	<4.5	45	<1.04	160
Average		**6,800**	**6,200**			**2,000**	**1,500**	**3,900**	**220**	**1,000**	**3.0**	**48**	**0.61**	**130**
1 σ (RSD)		**260 (4%)**	**1,700 (27%)**			**260 (13%)**	**510 (35%)**	**580 (15%)**	**54 (24%)**	**240 (23%)**	**1.2 (40%)**	**11 (23%)**	**0.28 (46%)**	**22 (16%)**

Table 7. Analyzed atomic ratios and errors of Cl/Na, Br/Na, and 1'000*Br/Cl in natural brine inclusion assemblages. The assemblages are from quartz veins of several mineral deposits at El Teniente (Cu-Mo-Au; Chile), Bingham Canyon (Cu-Mo-Au; USA), and Mole Granite (Sn-W; Austrailia). Scapolite mineral (Sca17) was employed as an external standard for the quantifications of Br/Cl ratios in the brine inclusions.

	Inclusion size(µm)	*Cl/Na	Error: 1σ of Cl/Na (% RSD)	*Br/Na	Error: 1σ of Br/Na (% RSD)	*1,000·(Br/Cl)	1σ of 1,000·Br/Cl (% RSD)
Brine assemblage, Quartz-Molybdenite vein (JH2), Bingham Canyon Cu-Mo-Au deposit							
10ma28c05	30	2.50	0.007 (0.3%)	0.0110	0.00020 (1.8%)	4.20	0.09 (2.1%)
10ma28c06	60	2.40	0.003 (0.1%)	0.0089	0.00005 (0.5%)	3.80	0.02 (0.7%)
10ma28c07	30	2.80	0.008 (0.2%)	0.0120	0.00022 (1.9%)	4.10	0.09 (2.1%)
10ma28c09	45	2.30	0.005 (0.2%)	0.0079	0.00009 (1.1%)	3.50	0.05 (1.3%)
10ma28c10	40	2.50	0.007 (0.3%)	0.0089	0.00014 (1.6%)	3.60	0.07 (1.9%)
10ma28c11	40	2.70	0.009 (0.3%)	0.0095	0.00019 (2.0%)	3.60	0.08 (2.3%)
10ma28c13	35	2.70	0.006 (0.2%)	0.0120	0.00012 (1.0%)	4.40	0.05 (1.2%)
Average		**2.56**		**0.0100**		**3.90**	
1 σ (RSD)		**0.18 (7%)**		**0.0016 (16%)**		**0.36 (9%)**	
Brine assemblage, Quartz-Anhydrite vein (2212-355), El Teniente Cu-Mo-Au deposit							
10ap20a10	30	2.10	0.007 (0.3%)	0.0088	0.00018 (2.0%)	4.30	0.10 (2.3%)
10ap20a11	45	2.00	0.005 (0.2%)	0.0088	0.00011 (1.2%)	4.30	0.06 (1.4%)
10ap20a12	30	2.10	0.005 (0.3%)	0.0084	0.00015 (1.8%)	3.90	0.08 (2.1%)
10ap20a13	20	2.00	0.008 (0.4%)	0.0080	0.00023 (2.8%)	4.00	0.13 (3.2%)
10ap20a14	30	2.00	0.004 (0.2%)	0.0084	0.00008 (0.9%)	4.30	0.05 (1.1%)
10ap20a16	30	2.10	0.006 (0.3%)	0.0083	0.00016 (1.9%)	3.90	0.09 (2.2%)
10ap20a18	50	1.90	0.003 (0.2%)	0.0070	0.00009 (1.3%)	3.70	0.06 (1.5%)
10ap20a20	30	2.10	0.006 (0.3%)	0.0090	0.00011 (1.2%)	4.30	0.07 (1.5%)
Average		**2.04**		**0.0083**		**4.10**	
1 σ (RSD)		**0.07 (4%)**		**0.0006 (8%)**		**0.22 (5%)**	
Brine assemblage, Quartz Sn-W vein, Yankee Lode (Y1), Mole Granite Sn-W deposit							
10ma20d05	30	2.70	0.008 (0.3%)	0.0058	0.00014 (2.4%)	2.10	0.06 (2.7%)
10ma20d08	75	2.60	0.002 (0.1%)	0.0055	0.00003 (0.5%)	2.10	0.01 (0.6%)
10ma20d09	50	2.60	0.004 (0.2%)	0.0053	0.00005 (0.9%)	2.00	0.02 (1.0%)
10ma20d12	75	2.60	0.003 (0.1%)	0.0051	0.00003 (0.5%)	2.00	0.01 (0.6%)
10ma20d13	35	3.00	0.005 (0.2%)	0.0060	0.00007 (1.1%)	1.90	0.02 (1.3%)
10ma20d14	35	3.10	0.006 (0.2%)	0.0060	0.00008 (1.4%)	1.90	0.03 (1.5%)
10ma20d15	40	2.40	0.006 (0.2%)	0.0048	0.00009 (1.9%)	1.90	0.04 (2.1%)
Average		**2.71**		**0.0055**		**2.00**	
1 σ (RSD)		**0.25 (9%)**		**0.0005 (8%)**		**0.08 (4%)**	

* atomic ratios, employed Sca17 external standard

4. Conclusion

We determined the precisions and accuracies of in-situ laser ablation ICP-MS microanalysis of sulfur, chlorine, and bromine in single fluid inclusions and conclude that careful contamination control and instrument optimization allows accuracies and precisions that are adequate for many geochemical applications. Precisions and accuracies of the anion analyses depend primarily on fluid inclusion size, fluid density, and optimized baseline blanks. Precisions of sulfur were found in the range of 17 - 44%, and bromine/chlorine ratios within 6 - 26% RSD in relatively small synthetic fluid inclusion assemblages, but were more precise within 4 - 9% in natural assemblages of large brine inclusions. Limits of detection of sulfur, chlorine, and bromine of 25-35 µm sized liquid inclusion are 160 ± 110

μg/g, 340 ± 220 μg/g, and 17 ± 10 μg/g, respectively. For reliable sulfur analysis, repeated cleaning of the ablation chamber with careful host background corrections of transient signals are critical, to minimize the effect of S background caused by UV remobilization of S contamination from inner surfaces of the ablation chamber. Applications show that sulfur can be quantified even in low density vapor inclusions. The measurement of Br/Cl ratios can be used to distinguish high density fluid inclusions from different deposit types, even in texturally complex samples where bulk leaching is impractical.

Acknowledgements

We thank Wim Malfait for Br-glass synthesis and RBS measurement, Jessica Langlade for EPMA analyses, Andreas Audétat for afghanite minerals and EPMA analyses, and Markus Wälle for the consistent support for LA-ICP-MS analyses. This research was funded by Swiss NSF Grant 200020-116693/1 for JHS and PBEZ2-118876 for ZZ. It was also supported by a Marie Curie International Outgoing Fellowship (no. 221054) within the 7th European Community Framework Program for ZZ. We thank Larryn Diamond for review.

References

Baker, T. et al., 2008. Mixed messages in iron oxide-copper-gold systems of the Cloncurry district, Australia: insights from PIXE analysis of halogens and copper in fluid inclusions. Mineralium Deposita, 43(6): 599-608.

Balcone-Boissard, H., Villemant, B. and Boudon, G., 2010. Behavior of halogens during the degassing of felsic magmas. Geochemistry Geophysics Geosystems, in press.

Banks, D.A. and Yardley, B.W.D., 1992. Crush-leach analysis of fluid inclusions in small natural and synthetic samples. Geochimica Et Cosmochimica Acta, 56(1): 245-248.

Bohlke, J.K. and Irwin, J.J., 1992a. Brine history indicated by argon, krypton, chlorine, bromine, and iodine analyses of fluid inclusions from the Mississippi Valley type lead fluorite barite deposits ar Hansonburg, New-Mexico. Earth and Planetary Science Letters, 110(1-4): 51-66.

Bohlke, J.K. and Irwin, J.J., 1992b. Laser microprobe analyese of noble-gas isotopes and halogens in fluid inclusions - Analyses of microstandards and synthetic inclusions in quartz. Geochimica Et Cosmochimica Acta, 56(1): 187-201.

Braitsch, O., 1971. Salt deposits; their origin and composition. Springer-Verlag.

Bray, C.J. and Spooner, E.T.C., 1992. Fluid inclusion volatile analysis by gas-chromatography with photoionization micro-thermal conductivity detectors - applications to magmatic MoS2 and other H2O-CO2 and H2O-CH4 fluids. Geochimica et Cosmochimica Acta, 56(1): 261-272.

Bureau, H. and Metrich, N., 2003. An experimental study of bromine behaviour in water-saturated silicic melts. Geochimica et Cosmochimica Acta, 67(9): 1689-1697.

Burgess, R., Layzelle, E., Turner, G. and Harris, J.W., 2002. Constraints on the age and halogen composition of mantle fluids in Siberian coated diamonds. Earth and Planetary Science Letters, 197(3-4): 193-203.

Cauzid, J., Philippot, P., Martinez-Criado, G., Menez, B. and Laboure, S., 2007. Contrasting Cu-complexing behaviour in vapour and liquid fluid inclusions from the Yankee Lode tin deposit, Mole Granite, Australia. Chemical Geology, 246(1-2): 39-54.

Crerar, D.A. and Barnes, H.L., 1976. Ore soulution chemistry 5. Solubilities of chalcopyrite and chalcocite assemblages in hydrothermal soultion at 200 deg to 350 deg C. Economic Geology, 71(4): 772-794.

Davis, S.N., Whittemore, D.O. and Fabryka-Martin, J., 1998. Uses of chloride/bromide ratios in studies of potable water. Ground Water, 36(2): 338-350.

Driesner, T. and Heinrich, C.A., 2007. The system H_2O-NaCl. Part I: Correlation formulae for phase relations in temperature-pressure-composition space from 0 to 1000 ^{0}C, 0 to 5000 bar, and 0 to 1 X-NaCl. Geochimica et Cosmochimica Acta, 71(20): 4880-4901.

Etschmann, B.E. et al., 2010. An in situ XAS study of copper(I) transport as hydrosulfide complexes in hydrothermal solutions (25–592 °C, 180–600 bar): Speciation and solubility in vapor and liquid phases. Geochimica et Cosmochimica Acta, 74(16): 4723-4739.

Foriel, J. et al., 2004. Biological control of Cl/Br and low sulfate concentration in a 3.5-Gyr-old seawater from North Pole, Western Australia. Earth and Planetary Science Letters, 228(3-4): 451-463.

Guillong, M. and Heinrich, C.A., 2007. Sensitivity enhancement in laser ablation ICP-MS using small amounts of hydrogen in the carrier gas. Journal of Analytical Atomic Spectrometry, 22(12): 1488-1494.

Guillong, M., Latkoczy, C., Seo, J.H., Günther, D. and Heinrich, C.A., 2008a. Determination of sulfur in fluid inclusions by laser ablation ICP-MS. Journal of Analytical Atomic Spectrometry, 23(12): 1581-1589.

Guillong, M., Meier, D.L., Allan, M.M., Heinrich, C.A. and Yardley, B.W.D., 2008b. SILLS: A MATLAB-based program for the reduction of laser ablation ICP-MS data of homogeneous materials and inclusions. Mineralogical Association of Canada Short Course 40: 328-333.

Günther, D., Audétat, A., Frischknecht, R. and Heinrich, C.A., 1998. Quantitative analysis of major, minor and trace elements in fluid inclusions using laser ablation inductively coupled plasma mass spectrometry. Journal of Analytical Atomic Spectrometry, 13(4):

263-270.

Günther, D., Frischknecht, R., Heinrich, C.A. and Kahlert, H.J., 1997. Capabilities of an Argon Fluoride 193 nm excimer laser for laser ablation inductively coupled plasma mass spectrometry microanalysis of geological materials. Journal of Analytical Atomic Spectrometry, 12(9): 939-944.

Halter, W.E., Pettke, T. and Heinrich, C.A., 2004. Laser-ablation ICP-MS analysis of silicate and sulfide melt inclusions in an andesitic complex I: analytical approach and data evaluation. Contributions to Mineralogy and Petrology, 147(4): 385-396.

Halter, W.E., Pettke, T., Heinrich, C.A. and Rothen-Rutishauser, B., 2002. Major to trace element analysis of melt inclusions by laser-ablation ICP-MS: methods of quantification. Chemical Geology, 183(1-4): 63-86.

Heinrich, C.A., Bain, J.H.C., Fardy, J.J. and Waring, C.L., 1993. Br/Cl geochemistry of hydrothermal brines associated with Proterozoic metasediment-hosted copper mineralization at Mount Isa, northwestern Australia. Geochimica et Cosmochimica Acta, 57(13): 2991-3000.

Heinrich, C.A., Driesner, T., Stefansson, A. and Seward, T.M., 2004. Magmatic vapor contraction and the transport of gold from the porphyry environment to epithermal ore deposits. Geology, 32(9): 761-764.

Heinrich, C.A. et al., 2003. Quantitative multi-element analysis of minerals, fluid and melt inclusions by laser-ablation inductively-coupled-plasma mass-spectrometry. Geochimica et Cosmochimica Acta, 67(18): 3473-3497.

Heinrich, C.A., Ryan, C.G., Mernagh, T.P. and Eadington, P.J., 1992. Segregation of ore metals between magmatic brine and vapor - A fluid inclusion study using PIXE microanalysis. Economic Geology, 87(6): 1566-1583.

Holser, W.T., 1983. Trace elements and isotopes in evaporites. In: R.G. Burns (Editor), Marine Minerals, Rev. Mineral. Mineralogical Society of America, pp. 295-346.

Jambon, A., Deruelle, B., Dreibus, G. and Pineau, F., 1995. Chlorine and bromine abundance in MORB: The contrasting behaviour of the Mid-Atlantic Ridge and East Pacific Rise and implications for chlorine geodynamic cycle. Chemical Geology, 126(2): 101-117.

Kharaka, Y.K. et al., 1987. Geochemistry of metal-rich brines from central Mississippi Valley Salt Dome basin. USA. Applied Geochemistry, 2: 543-561.

Liebscher, A., Luders, V., Heinrich, W. and Schettler, G., 2006. Br/Cl signature of hydrothermal fluids: liquid-vapour fractionation of bromine revisited. Geofluids, 6(2): 113-121.

Nagaseki, H. and Hayashi, K.I., 2008. Experimental study of the behavior of copper and zinc in a boiling hydrothermal system. Geology, 36(1): 27-30.

Nahnybida, T., Gleeson, S.A., Rusk, B.G. and Wassenaar, L.I., 2009. Cl/Br ratios and stable chlorine isotope analysis of magmatic-hydrothermal fluid inclusions from Butte, Montana and Bingham Canyon, Utah. Mineralium Deposita, 44(8): 837-848.

Ohmoto, H. and Lasaga, A.C., 1982. Kinetics of reactions between aqueous sulfates and sulfides in hydrothermal systems. Geochimica et Cosmochimica Acta, 46(10): 1727-1745.

Pettke, T., Heinrich, C.A., Ciocan, A.C. and Günther, D., 2000. Quadrupole mass spectrometry and optical emission spectroscopy: detection capabilities and representative sampling of short transient signals from laser-ablation. Journal of Analytical Atomic Spectrometry, 15(9): 1149-1155.

Pettke, T., Oberli, F. and Heinrich, C.A., 2010. The magma and metal source of giant porphyry-type ore deposits, based on lead isotope microanalysis of individual fluid inclusions. Earth and Planetary Science Letters, 296(3-4): 267-277.

Pokrovski, G.S., Borisova, A.Y. and Harrichoury, J.C., 2008. The effect of sulfur on vapor-liquid fractionation of metals in hydrothermal systems. Earth and Planetary Science Letters, 266(3-4): 345-362.

Ryan, C.G., Heinrich, C.A. and Mernagh, T.P., 1993. PIXE microanalysis of fluid inclusions and its application to study ore metal segregation between magmatic brine and vapor. Nuclear Instruments & Methods in Physics Research Section B-Beam Interactions with Materials and Atoms, 77(1-4): 463-471.

Seo, J.H., Guillong, M. and Heinrich, C.A., 2009. The role of sulfur in the formation of magmatic-hydrothermal copper-gold deposits. Earth and Planetary Science Letters, 282: 323-328.

Seward, T.M. and Barnes, H.L., 1997. Metal transport by hydrothermal ore fluids. Geochemistry of hydrothermal ore deposits, 3rd edition, 435-486. Wiley.

Skewes, M.A., Arevalo, A., Floody, R., Zuniga, P.H. and Stern, C.R., 2002. The giant El Teniente breccia deposit: Hypogene copper distribution and emplacement. Society of Economic Geologist Special Publication, 9: 299-332.

Stefansson, A. and Seward, T.M., 2004. Gold(I) complexing in aqueous sulphide solutions to 500 degrees C at 500 bar. Geochimica et Cosmochimica Acta, 68(20): 4121-4143.

Stoffell, B., Appold, M.S., Wilkinson, J.J., McClean, N.A. and Jeffries, T.E., 2008. Geochemistry and Evolution of Mississippi Valley-Type Mineralizing Brines from the Tri-State and Northern Arkansas Districts Determined by LA-ICP-MS Microanalysis of Fluid Inclusions. Economic Geology, 103(7): 1411-1435.

Sumino, H. et al., 2010. Seawater-derived noble gases and halogens preserved in exhumed mantle wedge peridotite. Earth and Planetary Science Letters (294): 163-172.

Van Kranendonk, M.J., 2006. Volcanic degassing, hydrothermal circulation and the flourishing of early life on Earth: A review of the evidence from c. 3490-3240 Ma rocks of the Pilbara Supergroup, Pilbara Craton, Western Australia. Earth Science Reviews, 74(3-4): 197-240.

Villemant, B. and Boudon, G., 1999. H2O and halogen (F, Cl, Br) behaviour during shallow magma degassing processes. Earth and Planetary Science Letters, 168(3-4): 271-286.

Webster, J.D. and Mandeville, C.W., 2007. Fluid immiscibility in volcanic environments. In: A. Liebscher and C.A. Heinrich (Editors), Fluid-Fluid Interactions. Reviews in Mineralogy & Geochemistry, pp. 313-362.

Wilkinson, J.J., Everett, C.E., Boyce, A.J., Gleeson, S.A. and Rye, D.M., 2005. Intracratonic crustal seawater circulation and the genesis of subseafloor zinc-lead mineralization in the Irish orefield. Geology, 33(10): 805-808.

Wood, S.A. and Samson, I.M., 1998. Solubility of ore minerals and complexation of ore metals in hydrothermal solutions. Techniques in Hydrothermal Ore Deposits Geology, 10. Society of Economic Geologists.

Yardley, B.W.D., 2005. 100th Anniversary Special Paper: Metal concentrations in crustal fluids and their relationship to ore formation. Economic Geology, 100(4): 613-632.

Zajacz, Z. and Halter, W., 2009. Copper transport by high temperature, sulfur-rich magmatic vapor: Evidence from silicate melt and vapor inclusions in a basaltic andesite from the Villarrica volcano (Chile). Earth and Planetary Science Letters, 282(1-4): 115-121.

Zajacz, Z. et al., 2010. Alkali metals control the release of gold from volatile-rich magmas. Earth and Planetary Science Letters, 297: 50-56.